Supporting Information

Sodiation Kinetics of Metal Oxide Conversion Electrodes: a Comparative Study with Lithiation

Kai He[†], Feng Lin[‡], Yizhou Zhu[§], Xiqian Yu[#], Jing Li[†], Ruoqian Lin[†], Dennis Nordlund[‖], Tsu-Chien Weng[‖], Ryan M. Richards[⊥], Xiao-Qing Yang[#], Marca M. Doeff[‡], Eric A. Stach[†], Yifei Mo[§,*], Huolin L. Xin[†,*], and Dong Su[†,*]

[†]Center for Functional Nanomaterials, Brookhaven National Laboratory, Upton, New York 11973, USA.

[‡]Energy Storage and Distributed Resources Division, Lawrence Berkeley National Laboratory, Berkeley, CA 94720, USA.

[§]Department of Materials Science and Engineering, University of Maryland, College Park, MD 20742, USA.

[#]Chemistry Department, Brookhaven National Laboratory, Upton, New York 11973, USA.

[‖]Stanford Synchrotron Radiation Lightsource, SLAC National Accelerator Laboratory, Menlo Park, California 94025, USA.

[⊥]Department of Chemistry and Geochemistry, Materials Science Program, Colorado School of Mines, Golden, Colorado 80401, USA.

*E-mails: yfmo@umd.edu; hxin@bnl.gov; dsu@bnl.gov

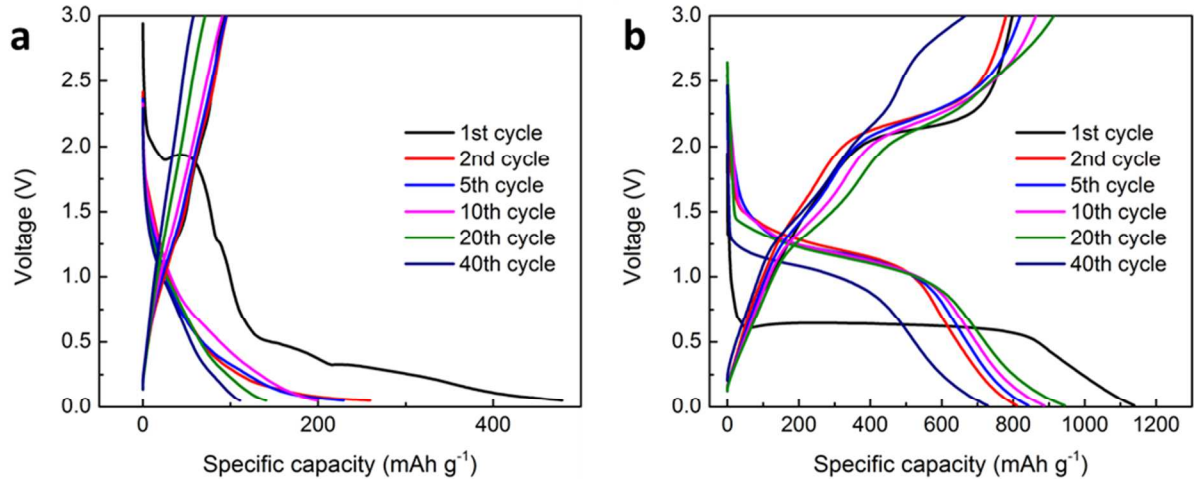

Figure S1. Charge-discharge profiles of different cycles for (a) Na half cell, and (b) Li half cell at rates of 0.1C.

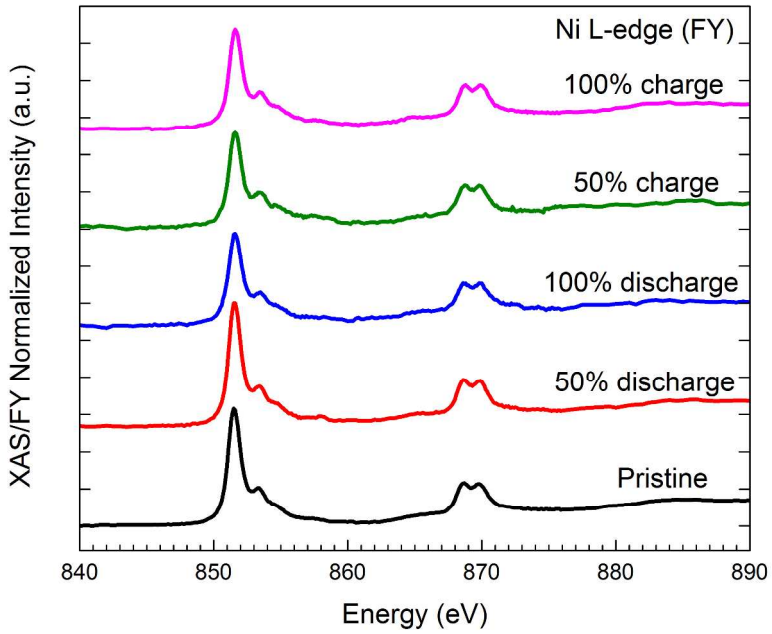

Figure S2. XAS spectra showing the normalized fluorescence yield (FY) intensity of the nickel L-edges in NiO electrodes at different SOC (0, 50%, 100% of the first discharge and 50% and 100% of first charge) in sodium half-cells. Note that the probing depth of FY is larger than the thickness of NiO nanosheets.

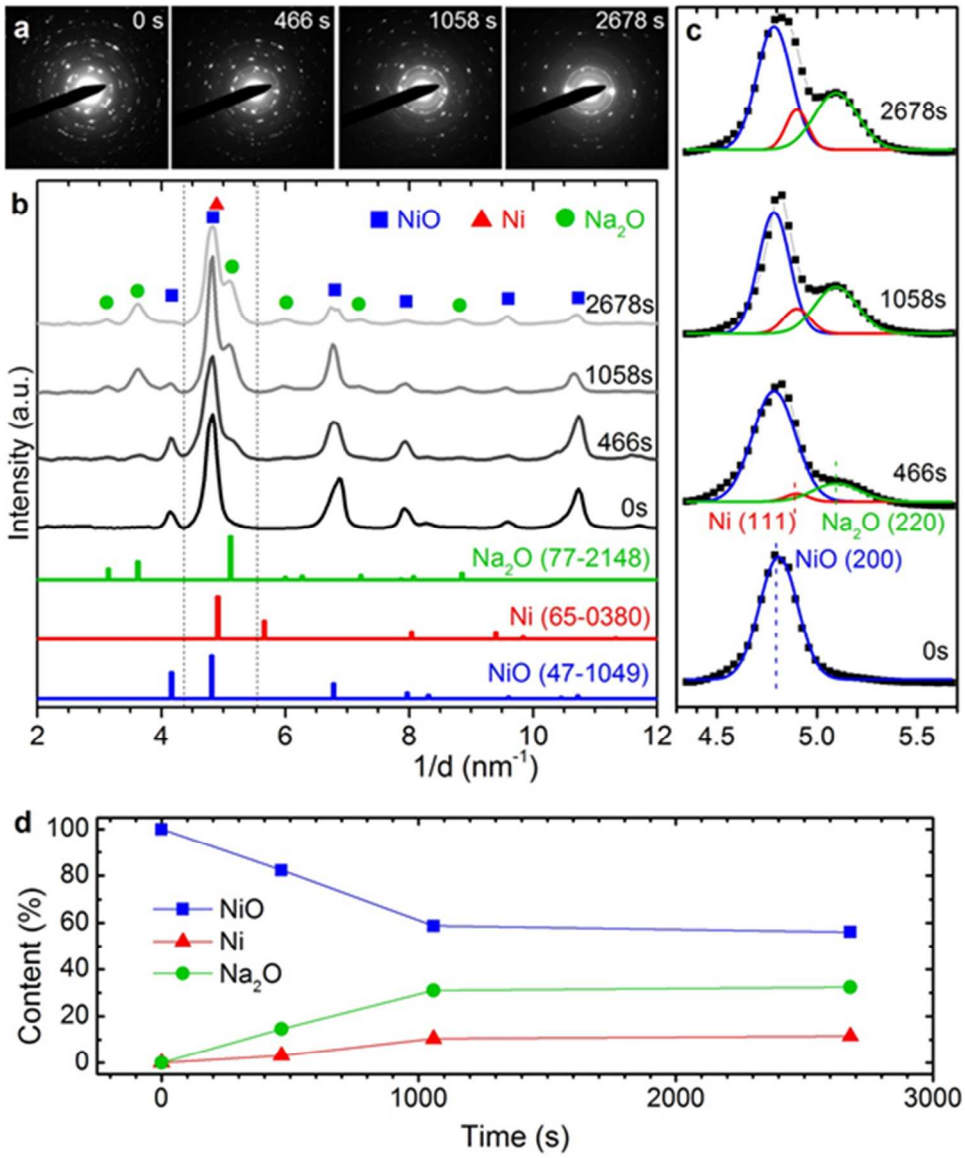

Figure S3. *In situ* electron diffraction during sodiation. (a) Electron diffraction patterns captured in real time (at 0 s, 466 s, 1058 s, and 2687 s, see Movie 3, Supporting Information) during in situ sodiation of NiO electrodes. (b) Rotationally integrated intensity profiles corresponding to the diffraction patterns in (a) with labeled peak assignments according to the standard JCPDS indexes indicated at the bottom. (c) The enlarged view of the major peaks between dotted lines in (b), which are decomposed into NiO (200), Ni (111), and Na_2O (220) reflections using linear combination of Gaussian fitting. (d) Relative content changes of each phase as a function of sodiation time.

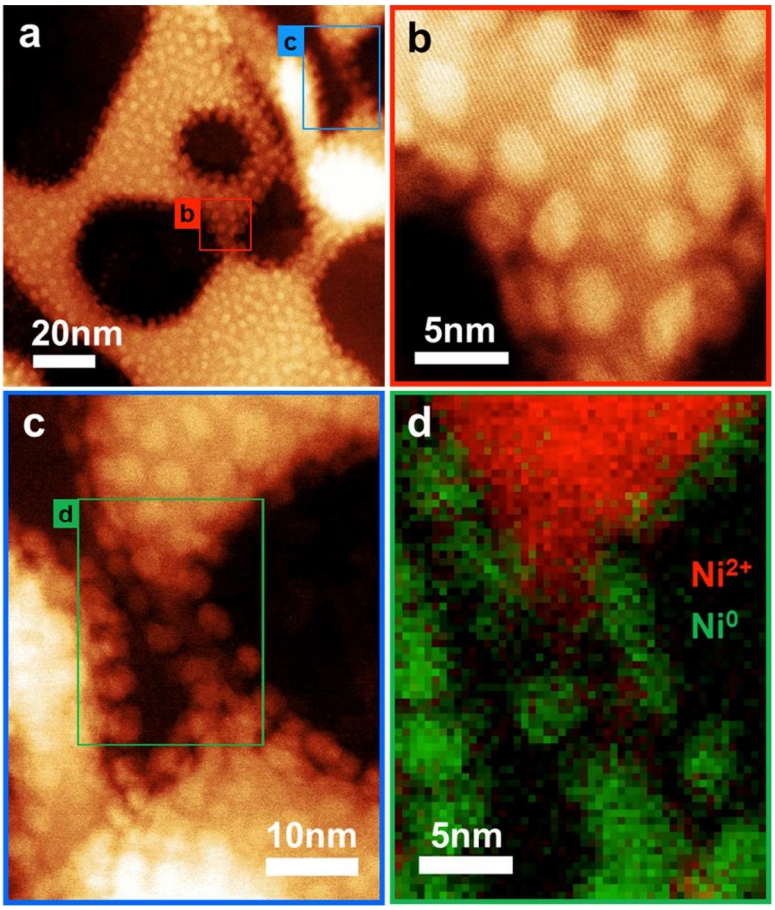

Figure S4. STEM imaging and EELS mapping. (a) STEM-ADF image of the NiO nanosheet after in situ sodiation. (b, c) The magnified views of the boxed areas in (a) showing reduced Ni nanoparticles (bright) covering the surface of the unreacted NiO nanosheet. (d) EELS mapping showing the valence charge distribution of Ni^{0} (green) and Ni^{2+} (red) in the boxed area in (c).

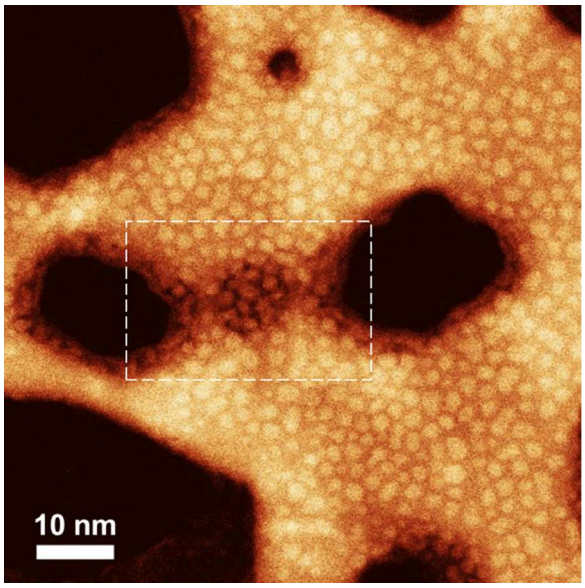

Figure S5. ADF-STEM image showing an in situ sodiated NiO nanosheet. The boxed region was selected for 3D visualization by STEM tomography corresponding to Figure 3d.

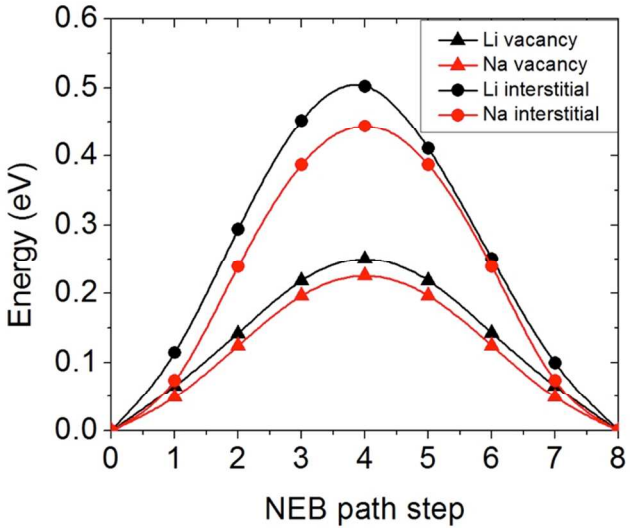

Figure S6. The NEB calculation results for the migration energy barrier of Li and Na in Li_2O and Na_2O, respectively. The migration energy barriers of Li in Li_2O are similar compared to Na in Na_2O.

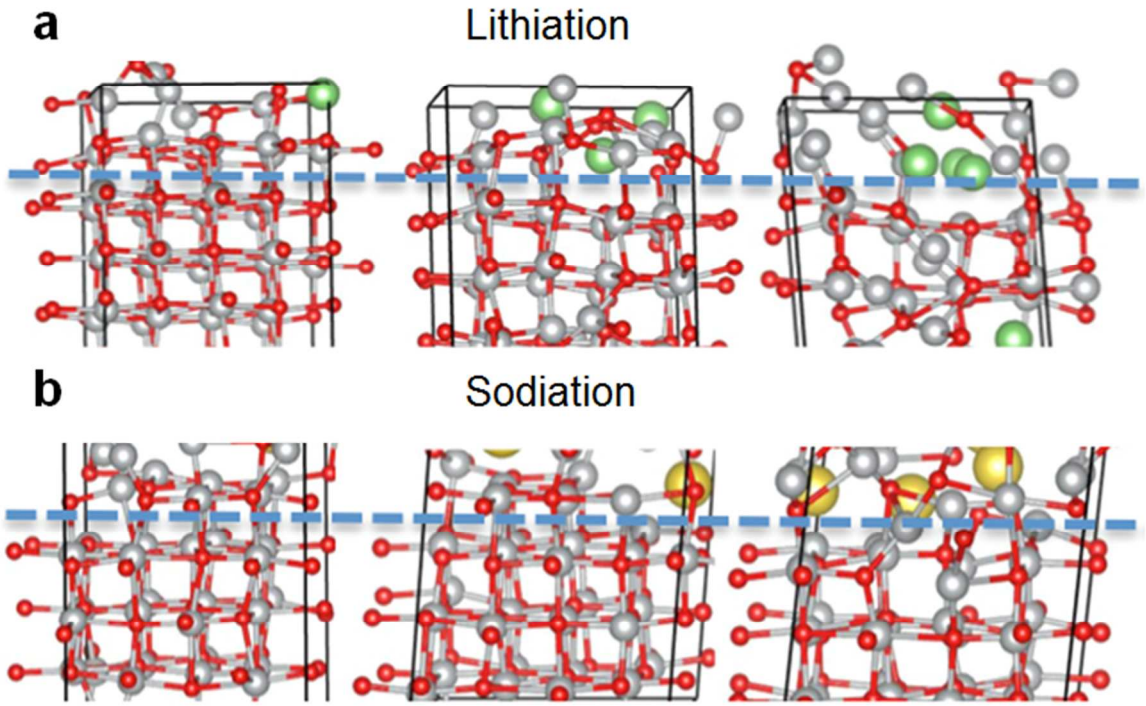

Figure S7. Snapthots from the AIMD simulations showing the layer-by-layer reaction mechanism in lithiation (a) and sodiation (b). The lithiation and sodiation proceeded through removing the NiO (001) layer, which took 6ps and 14ps for lithiation and sodiation, respectively. Dashed lines are for eye-guiding purpose.

Table S1. The formation energy of Li/Na vacancy/interstitial in Li_2O/Na_2O. The DFT calculations were performed in a 2×2×2 supercell model of Li_2O/Na_2O with one vacancy/interstitial of Li/Na. The defect formation energies were evaluated at the Li/Na chemical potential at the metallic states (μ_{Li_metal} = -1.91 eV and μ_{Na_metal} = -1.31 eV) and at the equilibrium potential ($\mu_{Li\_reaction}$ = -4.08 eV and $\mu_{Na\_reaction}$ = -2.56 eV) for the conversion reactions. The formation of Li/Na vacancies is energetically more favorable during the conversion reaction than the interstitials.

Host materials	Defect type	Defect formation energy (eV)		Migration Barrier (eV)
		At the metallic state	At the conversion potential	
Li_2O	Vacancy	3.38	1.21	0.25
Na_2O	Vacancy	2.20	0.95	0.22
Li_2O	Interstitial	3.13	5.30	0.50
Na_2O	Interstitial	1.27	2.52	0.44

Supporting Movies:

Movie 1. *In situ* TEM showing sodiation process *via* the shrinking-core mode. The movie is accelerated by 50 times.

Movie 2. *In situ* TEM showing lithiation process *via* the combination of shrinking-core and finger modes. The movie is accelerated by 30 times.

Movie 3. *In situ* electron diffraction during a sodiation process. The movie is accelerated by 100 times.

Movie 4. 3D STEM tomography of NiO after sodiation showing redox reaction occurring only on the surface NiO nanosheet.